Journal of Power Sources 413 (2019) 344–350

Contents lists available at ScienceDirect

Journal of Power Sources

journal homepage: www.elsevier.com/locate/jpowsour

Suppression of dendrites and granules in surface-patterned Li metal anodes using $CsPF_6$

Seokwoo Kim[a,1], Junyoung Choi[a,1], Hongkyung Lee[b], Yong-Cheol Jeong[c], Yong Min Lee[d,**], Myung-Hyun Ryou[a,*]

[a] Department of Chemical and Biological Engineering, Hanbat National University, 125 Dongseo-daero, Yuseong-gu, Daejeon, 34158, Republic of Korea
[b] Energy and Environment Directorate, Pacific Northwest National Laboratory, 902 Battelle Boulevard, Richland, WA, 99354, USA
[c] Micro/Nano Scale Manufacturing R&C Department, KITECH, Ansan, 426-910, Republic of Korea
[d] Department of Energy Systems Engineering, Daegu Gyeongbuk Institute of Science and Technology (DGIST), 333 Techno Jungang-Daero, Daegu, 42988, Republic of Korea

HIGHLIGHTS

- Cesium hexafluorophosphate was introduced to surface-patterned Li metal anodes.
- Cs^+ ions and patterned Li showed synergistic improvement in cycle performance.
- Cs^+ ions hindered the formation of granule and dendrites of patterned Li metal.
- Cs^+ ions stabilized the morphology of the surface-patterned Li metal anodes during cycling.

GRAPHICAL ABSTRACT

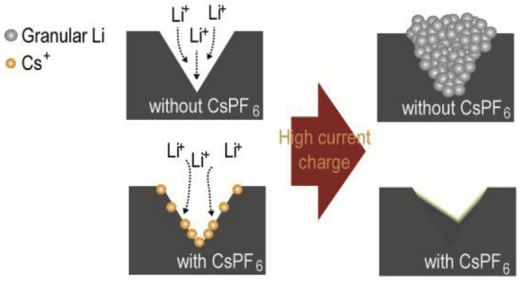

ARTICLE INFO

Keywords:
Lithium metal anodes
Cesium hexafluorophosphate
Lithium secondary batteries
Lithium dendrite
$CsPF_6$ additive

ABSTRACT

Unexpected Li deposition during plating, which causes low Coulombic efficiency and safety issues, limits the use of Li metal as an anode in commercial secondary batteries. With the recently developed micro-patterned Li metal anodes, dendrite formation during high current Li plating (2.4 mA cm^{-2}) has successfully been reduced, as Li ions are guided into the patterned holes. However, the uncontrolled formation of granular Li is still observed in this material. To overcome these shortcomings, we have introduced cesium hexafluorophosphate into micro-patterned Li metal anodes. This additive employs the self-healing electrostatic shield mechanism to effectively reduce the formation of granular Li and Li dendrites, thereby significantly improving the electrochemical performance of the anodes even when only small amounts (0.05 M) of electrolyte are used. Our experiments revealed that batteries employing surface-patterned Li metal anodes with cesium hexafluorophosphate maintained 88.7% (96.6 mAh g^{-1}) of their initial discharge capacity after the 900th cycle (Charging current density: C/2, 0.6 mA cm^{-2}, Discharging current density: 1C, 1.2 mA cm^{-2}), which is three times higher than the capacity observed with surface-patterned Li metal anodes without the additive (discharge capacity starts to decrease from 300 cycles).

* Corresponding author.
** Corresponding author.
E-mail address: mhryou@hanbat.ac.kr (M.-H. Ryou).
[1] Both authors contributed equally to this work.

https://doi.org/10.1016/j.jpowsour.2018.12.052
Received 27 June 2018; Received in revised form 6 November 2018; Accepted 18 December 2018
Available online 26 December 2018
0378-7753/

1. Introduction

Li-ion batteries (LIBs) have been widely recognized as suitable power sources for mobile electronic devices, such as laptops and mobile phones, since their first release in 1991 [1]. However, in recent years, there has been a growing demand for new secondary battery systems with higher energy densities and stable cycle performance, to meet the requirements of large-scale applications such as electric vehicles and energy storage systems. The energy density of commercial LIBs is approaching the theoretical limit dictated by the capacity of the anode and cathode materials used in these batteries, implying that new active electrode materials based on new chemistries are required to increase the energy density of secondary batteries [2].

Compared to graphite (372 mAh g^{-1}), which has been used as an active anode material for commercial LIBs, Li has a higher theoretical specific capacity (3860 mAh g^{-1}), a very low negative redox potential (−3.04 V versus the standard hydrogen electrode) and low density (0.59 g cm^{-3}) [1–5]. Because of these advantages, Li metal has been considered to be a promising anode material for secondary batteries for more than four decades.

However, the formation of uncontrolled structures during Li plating means that it has not been applied to commercial secondary batteries [1,6]. The generation of structures such as Li dendrites, mossy Li, and granular Li during Li plating results in a large morphological change rupturing the native and solid electrolyte interphase (SEI) layers of the anode, which adversely affects its electrochemical performance by consuming electrolytes [7–10]. Large amounts of liquid electrolytes are consumed in forming SEI layers on the newly exposed Li metal surface.

We previously reported that surface-patterned Li metal significantly inhibits dendrite formation at high current densities, i.e., 2.4 mA cm^{-2} [3,11]. As a result, anodes employing this material exhibit improved electrochemical performance compared with anodes with pristine Li metal. However, mossy Li and granular Li can still be observed in surface-patterned Li, as large structural changes are still experienced in the plating of the porous material. Avoiding porous Li plating is key to improving the electrochemical performance of surface-patterned Li metal anodes.

Of the many approaches studied to suppress uncontrolled Li plating, such as the use of protective coatings [12–14], Li host materials [15,16], and functional separators [4], functional electrolytes containing additives appear to be the most economical and efficient solution, as only a small amount of the additive (0.1–5 wt%) [17–23], is required to improve the electrochemical performance of Li secondary batteries. A functional electrolyte containing cesium ions (Cs^+) was recently proposed as a method for controlling Li plating, based on a self-healing electrostatic shield mechanism (SHES) [22,24]. According to these studies, low concentrations of Cs^+ ions exhibit a lower reduction potential than Li^+ ions, thereby forming a positively charged electrostatic shield around the initial growth tips of the protrusions. This shielding eliminates Li dendrite formation by forcing the deposition of Li^+ ions into regions adjacent to the protrusions.

To investigate the possible synergistic effect between surface-patterned Li and low concentrations of Cs^+ ions on the suppression of uncontrolled Li plating, we introduced an electrolyte solution containing a small amount of $CsPF_6$ (0.05 M) to surface-patterned Li metal anode, and evaluated the electrochemical performance of the unit cell ($LiMn_2O_4$/Li metal). Our experiments demonstrate that the Cs^+ ions inhibits the formation of mossy and granular Li on the surface-patterned Li metal during plating at high current densities (2.4 mA cm^{-2}) and enhances the cycle performance and rate capability of the unit cells.

2. Experimental

2.1. Materials

Lithium hexafluorophosphate ($LiPF_6$), propylene carbonate (PC), ethylene carbonate (EC), ethyl methyl carbonate (EMC), and dimethyl carbonate (DMC) were purchased from Enchem (Battery grade, Enchem Co., Ltd., Korea), and used as received. Cesium hexafluorophosphate ($CsPF_6$, > 99.0%, anhydrous) was ordered from SynQuest Laboratories, and dried at 60 °C for four days under vacuum, inside the antechamber of an argon-filled glove box. We prepared 1 M electrolyte solutions of $LiPF_6$ in a mixture of EC, PC, and EMC, at a weight ratio of 5:2:3, in the argon-filled glove box, with and without 0.05 M of $CsPF_6$. We used a microporous polyethylene (PE) membrane (ND420, Asahi Kasei E-Materials, Japan, porosity = 40%, thickness = 20 μm) as a battery separator.

We used $LiMn_2O_4$ (LMO, Iljin materials, Korea), conductive carbon (Super P Li®, Imerys, Belgium), polyvinylidene fluoride (PVDF, KF-1300, Kureha, M_w = 350,000), *N*-methyl-2-pyrrolidone (NMP, Sigma-Aldrich) and Al current collector foil (15 μm, Sam-A Aluminum) for the cathodes of the battery. The $LiMn_2O_4$ cathode was prepared by coating a slurry consisting of 90 wt% $LiMn_2O_4$, 5 wt% Super P Li®, and 5 wt% PVDF in NMP solvent onto a piece of Al foil using a doctor blade, and drying in an oven at 130 °C for 1 h (mass loading = 12 mg cm^{-2}, density = 1.8 mg cm^{-3}). The surface-patterned Li metal anode (200 μm, Honjo, Japan) was prepared as described in our previous work [11]. The 2032-coin type unit cells (LMO/Li metal) were assembled in the argon-filled glove box (dew point below −70 °C) by sandwiching the PE separator between the LMO and Li metal. We used 80 μL of electrolyte during battery assembly.

2.2. Characterization

The morphological features of the Li metal were analyzed using a field-emission scanning electron microscope (FE-SEM, S-4800, Hitachi, Japan) and a 3D digital microscope (VHX-900F, Keyence, Japan). To prepare the material for characterization, the unit cells (LMO/Li metal) were carefully disassembled in an argon-filled glove box, to detach the Li metal from the LMO. The Li metal was subsequently rinsed in DMC solvent, and dried under vacuum at 25 °C for 12 h, to remove the residual electrolyte on its surface. All the Li metal samples were packed into a hermetically-sealed Al polymer pack before SEM and digital microscope analysis, for safe transfer without contamination.

2.3. Electrochemical measurements

To initiate electrochemical characterization, we first define a series of processes consisting of formation and stabilization steps as precycling. The unit cells (LMO/Li metal) were cycled (formation step), i.e., charged and discharged, between 3.0 and 4.3 V relative to Li/Li^+, at C/10 (0.12 mA cm^{-2}), followed by three additional cycles (stabilization cycle) at C/5 (0.24 mA cm^{-2}). This precycling was conducted at 25 °C, in constant current (CC) mode, using a battery cycler (PNE Solution Co., LTD., Korea).

After precycling, the rate capability of the unit cells (LMO/Li metal) was evaluated by cycling between 3.0 and 4.3 V, relative to Li/Li^+, five times at different current densities. In these experiments, discharging was performed in CC mode, with the discharging current densities varied from C/2 to 20C (i.e., C/2, 1C, 2C, 3C, 5C, 7C, 10C, 15C, and 20C). Charging was performed in CC/constant voltage (CV) mode, with the current density maintained at C/2 (0.6 mA cm^{-2}). The cycling performance of the precycled unit cells was tested between 3.0 and 4.3 V relative to Li/Li^+ (charging: C/2 in CC/CV mode, discharging: 1C in CC mode) for 900 cycles at 25 °C.

To investigate the effect of $CsPF_6$ on the surface-patterned Li metal in the polarization process, 2032-type coin Li/Li symmetrical cells were

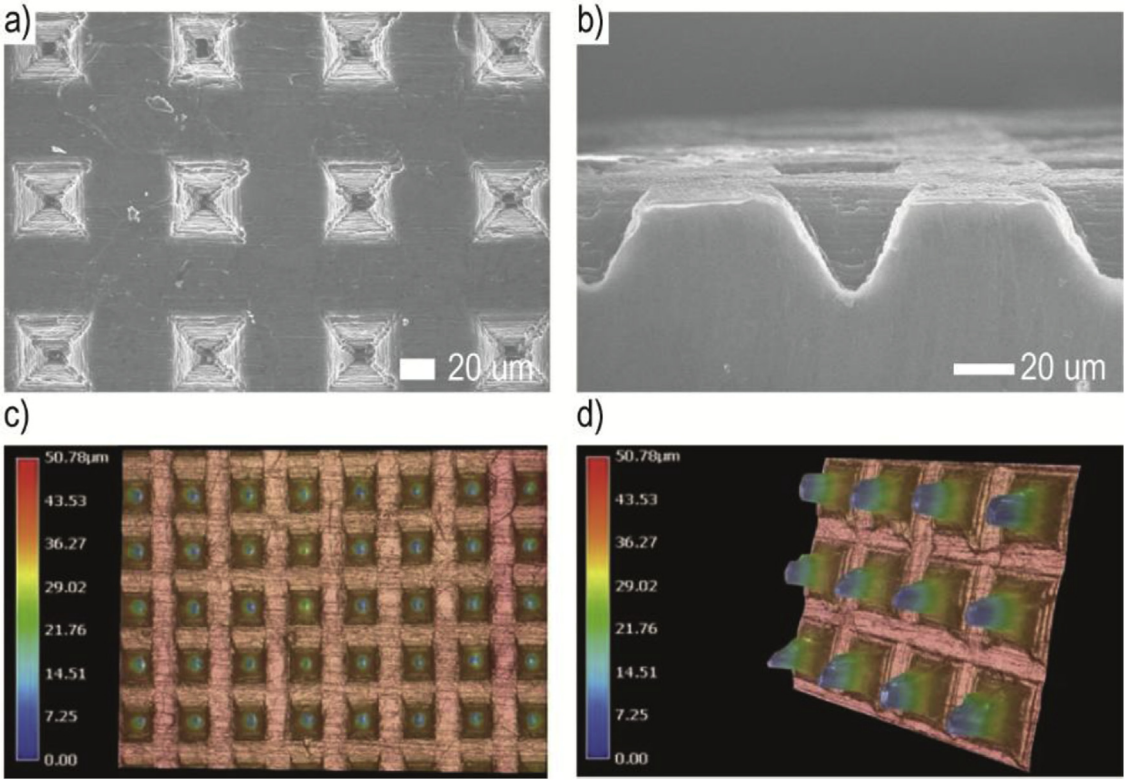

Fig. 1. (a: top view, b: cross-sectional view) SEM images of surface-patterned Li metal anodes. (c: top view, d: rotated view) Topographic images of the surface-patterned Li metal anodes obtained using 3D optical microscopy.

prepared, and Li plating and stripping experiments were performed at a current density of 2.4 mA cm^{-2}. Each cycle consisted of 5 min of plating, 10 min of rest, 5 min of stripping, and 10 min of rest. The rest time between the plating and stripping processes was selected to alleviate the effect produced by concentration gradients. Potential changes were monitored with respect to the reference Li electrode.

AC impedance measurements of the unit cells (LMO/Li metal) were conducted using a VSP impedance analyzer (Bio-Logic SAS, USA) in the frequency range from 1 MHz to 0.01 Hz.

3. Results and discussion

The morphology of the surface-patterned Li metal was observed using a combination of SEM (Fig. 1a and b) and 3D optical microscopy (OM) (Fig. 1c and d), to verify the reproducibility of the surface pattern over the entire area of the Li metal. Unlike SEM, with 3D OM a 3D image of a sample, which can be rotated and observed at any angle, is produced by combining OM images obtained from different focal planes. This technique allows more in-depth interrogation of the topology of the sample. In Fig. 1c and d, blue corresponds to the depth of the substrate, while red corresponds to its height. Based on 3D OM the inverted square pyramid has a height of 37.5 μm, a width of 40 μm, and a ridge length of 40 μm, which are in good agreement with the pattern dimensions estimated from the SEM images. The results of these characterizations suggest that periodic patterns were uniformly fabricated across the entire area of the surface of the Li metal.

We evaluated the cycle performance and rate capability of the unit cells (2032 coin-type cells, LMO/Li metal), to investigate the effects of $CsPF_6$ on their electrochemical properties. For simplicity, hereafter, we denote the unit cells containing and not containing $CsPF_6$ as Li metal with $CsPF_6$ and Li metal without $CsPF_6$, respectively.

The Li metal without $CsPF_6$ and the Li metal with $CsPF_6$ displayed similar potential profiles during precycling (Fig. 2, Li metal without $CsPF_6$: charge capacity = 108.7 mAh g^{-1}, discharge capacity = 107.9 mAh g^{-1}. Li metal with $CsPF_6$: charge capacity = 107.9 mAh g^{-1}, discharge capacity = 107.6 mAh g^{-1}). At 99.7%, the Li metal with $CsPF_6$ exhibited a slightly higher Coulombic efficiency (CE) than the Li metal without $CsPF_6$ (99.2%). Although the difference in the CE of the two systems (0.5%) seems small, it is enough to cause a big difference in the cycle performance and rate capability of the two types of unit cells. It thus appears that the effect of CE is compounded during cycling. The larger CE observed with the Li metal with $CsPF_6$ implies that $CsPF_6$ helps to form a more stable SEI layer on the surface-patterned Li metal during precycling. The surface chemical composition of the Li metal surface after precycling are summarized in Fig. S1 (Supplementary Materials).

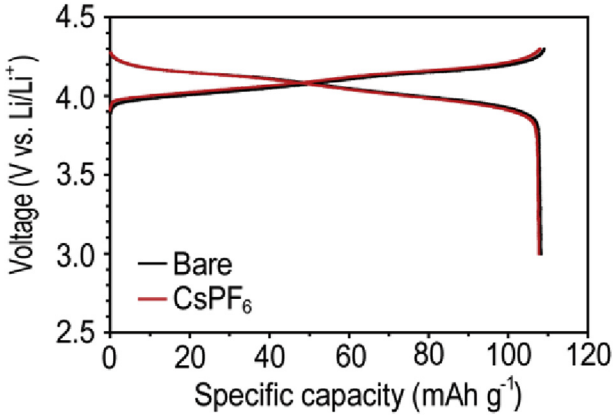

Fig. 2. Initial potential profiles of the unit cells (LMO/Li metal) containing the surface-patterned Li metal with and without $CsPF_6$.

The Li metal with $CsPF_6$ exhibited improved electrochemical performance compared to the Li metal without $CsPF_6$ (Fig. 3), as measured by the cycle life and rate capability tests. We observed a sharp decrease

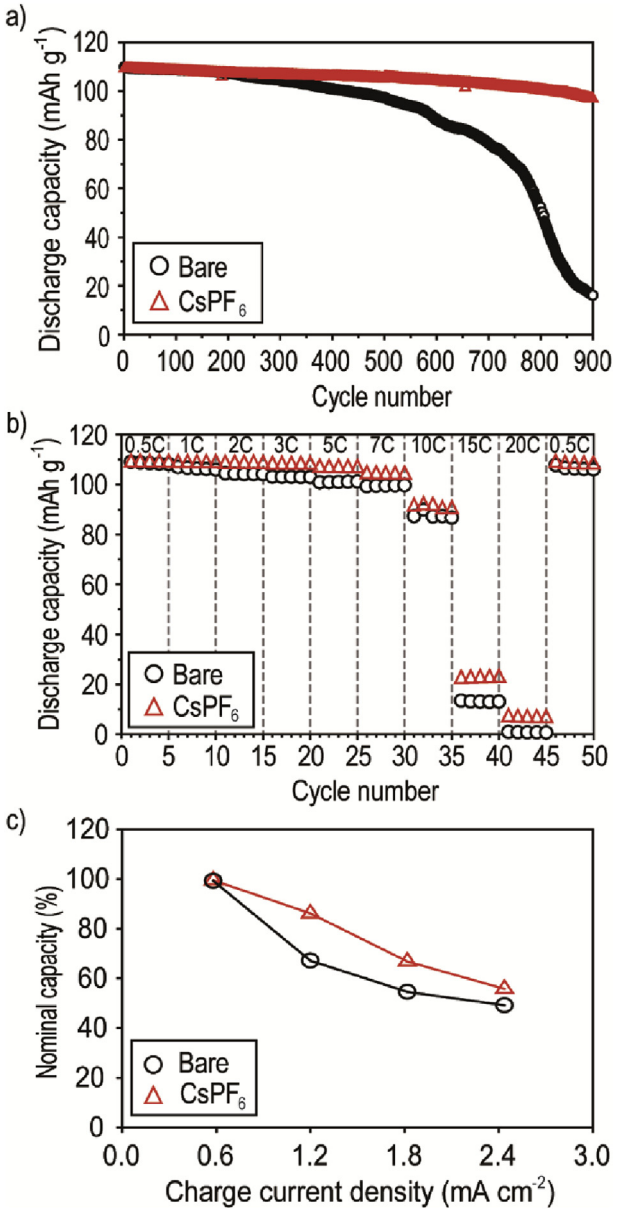

Fig. 3. Electrochemical performance of LMO/Li metal unit cells containing surface-patterned Li metal with and without $CsPF_6$. (a) Capacity of unit cells when cycling between 3.0 and 4.3 V relative to Li/Li^+ (charging rate = C/2 (0.6 mA cm^{-2}), discharging rate = 1C (1.2 mA cm^{-2})). (b) Rate capability determined by varying the discharging current from C/2 (0.6 mA cm^{-2}) to 20C (24.0 mA cm^{-2}), with the charging current fixed at C/2 (0.6 mA cm^{-2}). (c) Discharge capacity measured after the 100th cycle as a percentage of the initial discharge capacity measured during precycling (Fig. 2). In this experiment, the charging current for Li plating was varied from C/2 (0.6 mA cm^{-2}) to 2C (2.4 mA cm^{-2}), while the discharging current for Li stripping was fixed at 1C (1.2 mA cm^{-2}).

in the discharge capacity of the Li metal without $CsPF_6$ after 300 cycles, which eventually fell to 16.4 mAh g^{-1} (14.6% of its initial value) after 900 cycles. In contrast, the Li metal with $CsPF_6$ maintained a much higher discharge capacity of 96.6 mAh g^{-1} after 900 cycles (Fig. 3a). For analysis of the rate capability of the two types of cells, we studied two scenarios by comparing the capacity retention of both types of cells. In the first (Case 1, results shown in Fig. 3b), the charging (Li plating) rate was fixed and the discharging (Li stripping) rate was varied, while in the second (Case 2), the discharging rate was fixed and the charging rate was varied (Fig. 3c). We observed higher rate capabilities in the latter case than we did in the former. For instance, from Fig. 3b, which considers Case 1, we note that the Li metal with $CsPF_6$ displayed a capacity of 104.3 mAh g^{-1} after 30 cycles of discharging at 7 C (8.4 mA cm^{-2}), a value that is only 4% better than that obtained with the Li metal without $CsPF_6$ (99.7 mAh g^{-1} after 30 cycles of discharging at 7C). In contrast, for Case 2 (Fig. 3c), the Li metal with $CsPF_6$ exhibited a capacity of 94.4 mAh g^{-1} after charging at 1C (1.2 mA cm^{-2}), a value that is 28% better than that obtained with the Li metal without $CsPF_6$ (73.5 mAh g^{-1}). Based on these results, we can deduce that $CsPF_6$ plays a more important role in Li plating than it does in Li stripping. These results are in line with previous studies that the plating current density plays an important role in determining the cycle performance of Li metal anodes [4,9,11].

To elucidate the underlying mechanism dictating the improved cycle performance and rate capability of Li metal with $CsPF_6$, we investigated the interfacial resistance and morphological properties of surface-patterned Li metal treated with $CsPF_6$, using symmetric Li/Li cells and SEM.

In order to investigate the relationship between the electrochemical impedance and electrochemical performance of the unit cells in detail, we measured the potential profiles of symmetric cells, fabricated with surface-patterned Li, during galvanostatic Li plating/stripping (Fig. 4). This allows us to observe the role of Li metal more closely, while excluding the role of the LMO in the unit cell (LMO/Li metal) used in the electrochemical tests detailed in Fig. 3. The galvanostatic polarization experiments were conducted by applying a constant current for 1000 cycles in the following sequence: +2.4 mA cm^{-2} for 5 min → 10 min rest → −2.4 mA cm^{-2} for 5 min → 10 min rest. As the number of cycles increased, the symmetric cells composed of surface-patterned Li metal with $CsPF_6$ exhibited a smaller overpotential than the cells containing surface-patterned Li metal without $CsPF_6$. To illustrate the changes in overpotential observed with the two systems, a post-mortem analysis of the surface-patterned Li metal was performed using SEM, to observe the changes in morphology incurred during electrochemical testing.

To determine the effect of the $CsPF_6$ electrolyte additive on the patterned Li metal, we fabricated symmetric cells consisting of pristine and patterned Li. The same number of Li ions were plated on patterned Li metal with and without $CsPF_6$ (Li was plated for 5 min at 2.4 mA cm^{-2}, corresponding to 0.2 mAh). As detailed in our previous report [11], we observed uncontrolled granular Li structures in the micro-patterned holes of the Li metal without $CsPF_6$ (Fig. 5a–c). In contrast, with $CsPF_6$, the surface of the micro-patterned Li metal was stabilized (Fig. 5d–f), as the micro-patterned holes were filled with dense Li metal without the formation of uncontrolled Li structures such as dendrites, or mossy and granular Li. The suppression of granular Li

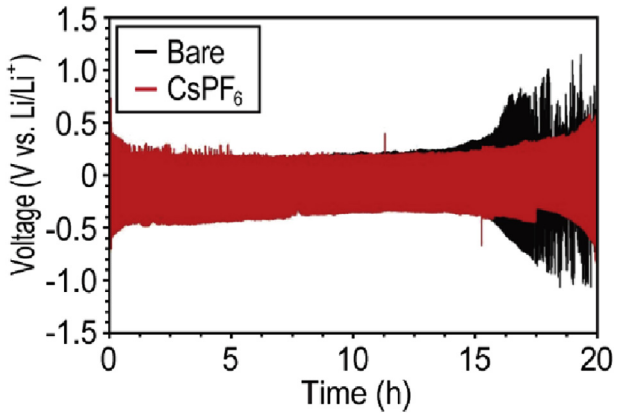

Fig. 4. Potential profiles of symmetric cells fabricated using surface-patterned Li with and without $CsPF_6$. Each polarization step was conducted by applying current in the following sequence: +2.4 mA cm^{-2} (5 min) → Rest (10 min) → −2.4 mA cm^{-2} (5 min) → Rest (10 min).

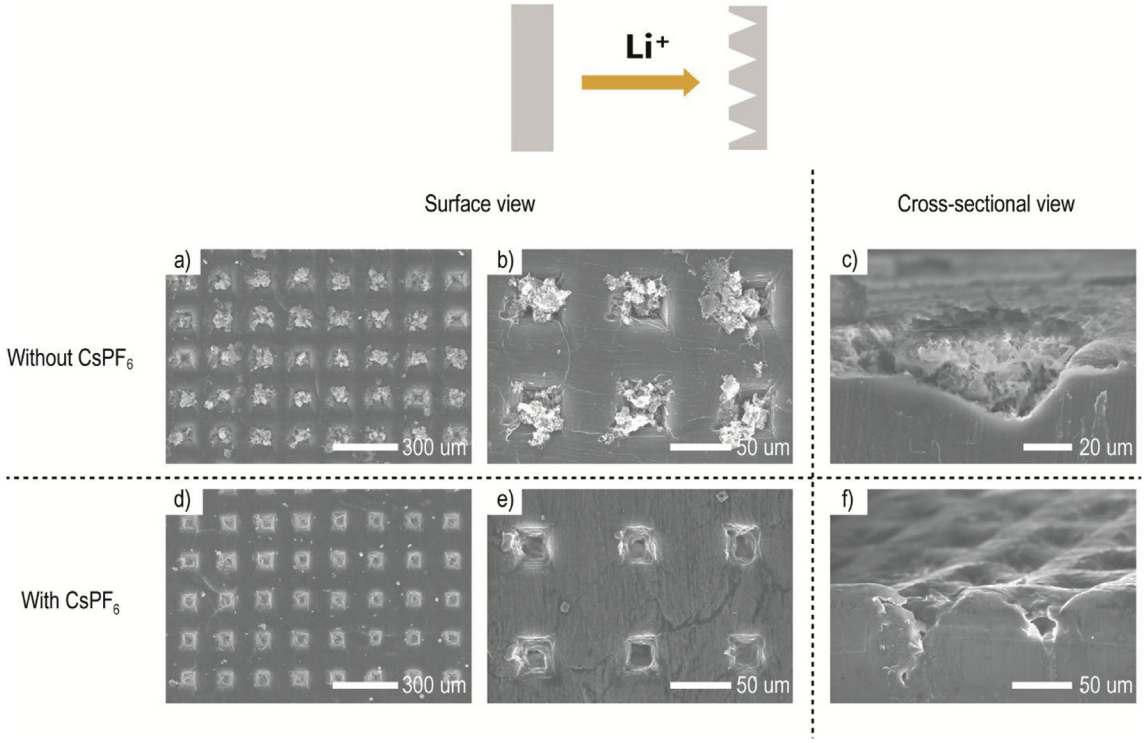

Fig. 5. The surface and cross-sectional SEM images of patterned Li metal (a–c) without $CsPF_6$, and (d–f) with $CsPF_6$, following moderate Li plating at 2.4 mA for 5 min (corresponding to 0.2 mAh).

by $CsPF_6$ is notable, as the generation of granular Li, which causes changes to the morphology of the Li metal surface resulting in the extra consumption of electrolytes in the formation SEI layer, was a limit to the efficacy of surface-patterned Li metal.

We further investigated the morphological changes to the surface-patterned Li metal in different Li plating conditions, corresponding to a capacity of 1.8 mAh. After precycling, as performed with the cells characterized in Fig. 2, the 2032 coin-type LMO/Li unit cells with and without $CsPF_6$ were disassembled, following additional charging and discharging, and the surface of the patterned Li metal was observed.

For both types of unit cells, the excess Li relative to the number of patterned holes meant that plated Li was deposited in these holes, as well as the ridge regions of the pattern (Fig. 6a–d). More importantly, the plated Li of the unit cell with $CsPF_6$ did not show a smooth surface morphology (Fig. 6c and d), an observation that contradicts the behavior reported in previous studies [22,24,25], where the SHES mechanism, activated by the use of $CsPF_6$, resulted in a smooth Li metal surface after plating. After discharging, the surface morphologies of the patterned Li metal with and without $CsPF_6$ were significantly different. For the Li metal without $CsPF_6$, Li ions were removed from the ridge region to create pits over the entire surface (Fig. 6e and f). In contrast, for the Li metal containing $CsPF_6$, Li ions were stripped from the bulky Li metal region, resulting in a smooth morphology (Fig. 6 g and h).

We conducted additional experiments to investigate the deviation in

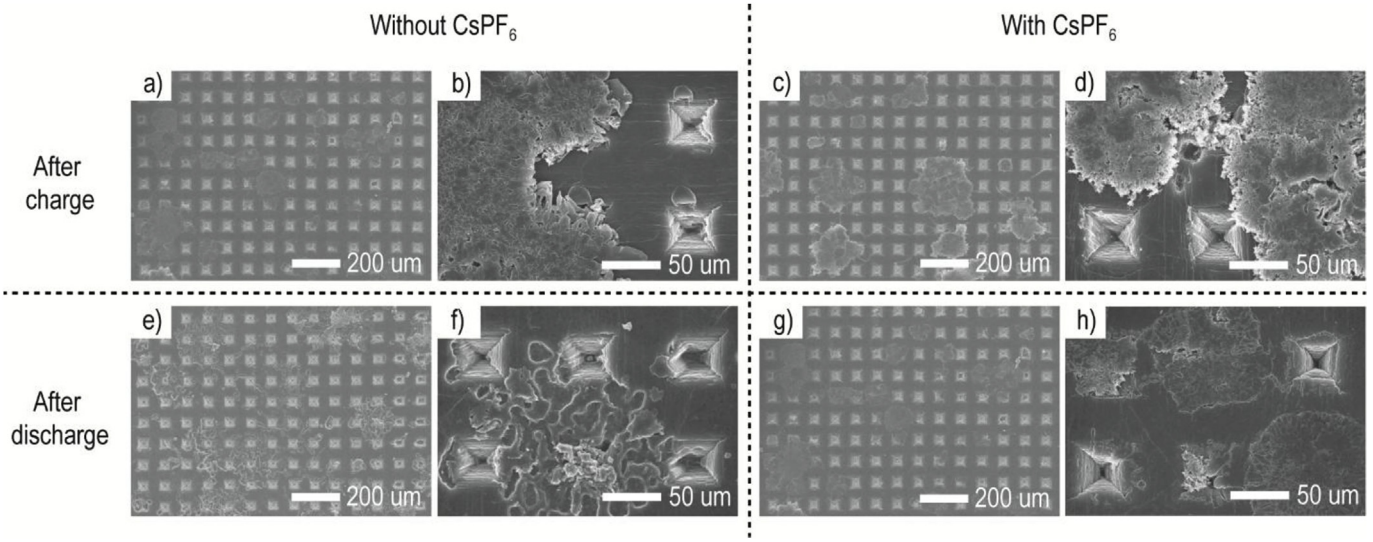

Fig. 6. SEM images of the surface-patterned Li metal after precycling (Li plating condition = 1.8 mAh). Effects of charging on samples (a and b) without $CsPF_6$, and (c and d) with $CsPF_6$. Effects of discharging on samples (e and f) without $CsPF_6$, and (g and h) with $CsPF_6$.

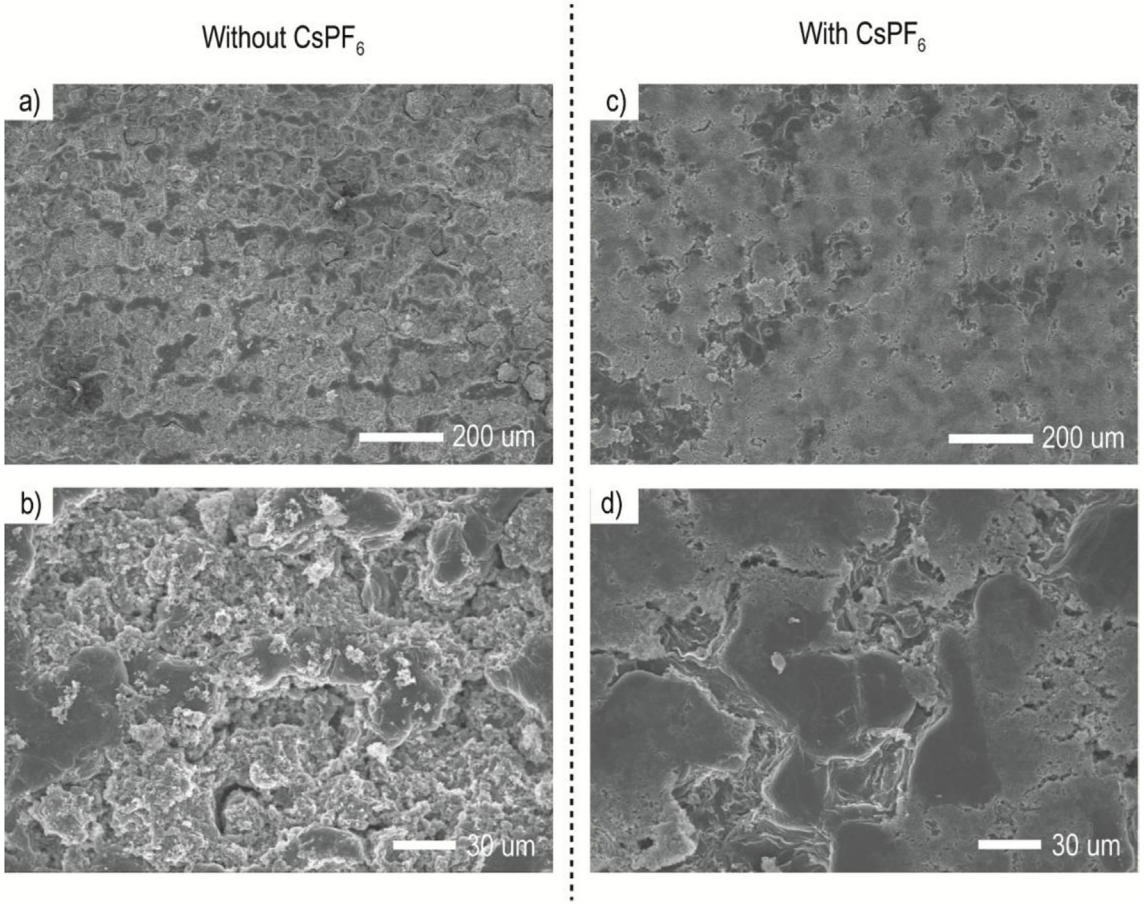

Fig. 7. SEM images of the surface-patterned Li metal (a and b) without $CsPF_6$, and (c and d) with $CsPF_6$, after 100 cycles corresponding to the characterizations in Fig. 3a.

the expected effect of $CsPF_6$ during charging. From the results of these experiments we can deduce that the amount of $CsPF_6$ electrolyte solution containing in the unit cells, and the number of Li ions during plating, play a significant role in determining the morphological structure of Li metal. As shown in Fig. S1 in the Supplementary Materials, a larger amount of liquid electrolyte (600 μL) resulted in a smoother Li metal surface compared with the morphology observed with a smaller amount of liquid electrolyte (80 μL). Moreover, by comparing the magnitude of Li plating (0.2 mAh and 1.8 mAh), we noticed that the surface-patterned Li metal exhibited a smooth Li surface following moderate Li plating (0.2 mAh, Fig. S2 in Supplementary Materials). The mechanism dictating these observations made during post-mortem analysis is under investigation and will be reported elsewhere.

The surface of the patterned Li metal was observed after 100 cycles, with conditions corresponding to those characterized in Fig. 3a. Similar to the results displayed in Fig. 6a, b, e, and f, the patterned Li metal without $CsPF_6$ had rough morphological features, as if the surface was torn off around the pattern (Fig. 7a and b). In contrast, the patterned Li metal with $CsPF_6$ exhibited a smoother surface (Fig. 7c and d). Based on the appearance of uncontrolled structures, which consume a large amount of electrolyte, we believe that the smoother surface of the patterned Li metal with $CsPF_6$ are an important reason for the significantly improved cycle performance of the unit cells characterized in Fig. 3a. This conclusion is supported by the results of impedance analysis, shown in Fig. S3 (Supplementary Materials). There was a large increase in the bulk resistance (R_b) of the Li metal without $CsPF_6$ (from 4.33 to 13.9 Ω) compared to that observed with the Li metal with $CsPF_6$ (from 2.43 to 3.55 Ω), implying that with the Li metal without $CsPF_6$, a larger amount of liquid electrolyte was consumed after cycling. The total resistance of the unit cells (R_{total}) is significantly influenced by the morphological characteristics of Li metal; for instance, the large surface area generated as a result of the formation of uncontrolled Li structures, reduce its magnitude, which confuses the exact interpretation of R_{total} [26–28]. Hence, we have avoided comparing R_{total} to determine the influence of electrolyte consumption on thick SEI formation.

4. Conclusion

Expecting a synergistic effect between the surface-patterned Li metal and $CsPF_6$, we introduced a 0.05 M $CsPF_6$ electrolyte solution to the surface-patterned Li metal. Although we did not observe the reported effects of the SHES mechanism (a smooth Li metal surface), as the relationship between the surface-patterned Li metal and $CsPF_6$ was more complex than envisaged, the additive still significantly stabilized the morphology of the surface-patterned Li metal in repeated Li plating/stripping, greatly improving cycle performance.

Acknowledgment

This work (Grants No. C0563844) was supported by Business for Cooperative R&D between Industry, Academy, and Research Institute funded Korea Small and Medium Business Administration in 20. This work was supported by the Basic Science Research Program through the National Research Foundation of Korea (NRF) funded by the Ministry of Education (NRF-2016R1D1A3B03933293). This research was supported by the Commercialization Promotion Agency for R&D Outcomes (COMPA) funded by the Ministry of Science and ICT(MSIT)

[2018K000154].

Appendix A. Supplementary data

Supplementary data to this article can be found online at https://doi.org/10.1016/j.jpowsour.2018.12.052.

References

[1] D. Lin, Y. Liu, Y. Cui, Reviving the lithium metal anode for high-energy batteries, Nat. Nanotechnol. 12 (3) (2017) 194 https://www.nature.com/articles/nnano.2017.16.

[2] J. Xiao, D. Mei, X. Li, W. Xu, D. Wang, G.L. Graff, W.D. Bennett, Z. Nie, L.V. Saraf, I.A. Aksay, Hierarchically porous graphene as a lithium–air battery electrode, Nano Lett. 11 (11) (2011) 5071–5078 http://pubs.acs.org/doi/abs/10.1021/nl203332e.

[3] M.H. Ryou, Y.M. Lee, Y. Lee, M. Winter, P. Bieker, Mechanical surface modification of lithium metal: towards improved Li metal anode performance by directed Li plating, Adv. Funct. Mater. 25 (6) (2015) 834–841 http://onlinelibrary.wiley.com/doi/10.1002/adfm.201402953/full.

[4] M.H. Ryou, D.J. Lee, J.N. Lee, Y.M. Lee, J.K. Park, J.W. Choi, Excellent cycle life of lithium-metal anodes in lithium-ion batteries with mussel-inspired polydopamine-coated separators, Adv. Energy Mater. 2 (6) (2012) 645–650 http://onlinelibrary.wiley.com/doi/10.1002/aenm.201100687/full.

[5] J.-M. Tarascon, M. Armand, Issues and challenges facing rechargeable lithium batteries, Nature 414 (2001) 359–367 https://www.nature.com/articles/35104644.

[6] D. Wang, W. Zhang, W. Zheng, X. Cui, T. Rojo, Q. Zhang, Towards high-safe lithium metal anodes: suppressing lithium dendrites via tuning surface energy, Adv. Sci. 4 (1) (2017) 1600168 http://onlinelibrary.wiley.com/doi/10.1002/advs.201600168/full.

[7] S. Shiraishi, K. Kanamura, Z.-i. Takehara, Imaging for uniformity of lithium metal surface using tapping mode-atomic force and surface potential microscopy, J. Phys. Chem. B 105 (1) (2001) 123–134 http://pubs.acs.org/doi/abs/10.1021/jp002014x.

[8] L. Gireaud, S. Grugeon, S. Laruelle, B. Yrieix, J.-M. Tarascon, Lithium metal stripping/plating mechanisms studies: a metallurgical approach, Electrochem. Commun. 8 (10) (2006) 1639–1649 https://www.sciencedirect.com/science/article/pii/S1388248106003092.

[9] D. Aurbach, E. Zinigrad, Y. Cohen, H. Teller, A short review of failure mechanisms of lithium metal and lithiated graphite anodes in liquid electrolyte solutions, Solid State Ionics 148 (3–4) (2002) 405–416 https://www.sciencedirect.com/science/article/pii/S0167273802000802.

[10] P. Bai, J. Li, F.R. Brushett, M.Z. Bazant, Transition of lithium growth mechanisms in liquid electrolytes, Energy Environ. Sci. 9 (10) (2016) 3221–3229 http://pubs.rsc.org/-/content/articlehtml/2016/ee/c6ee01674j.

[11] J. Park, J. Jeong, Y. Lee, M. Oh, M.H. Ryou, Y.M. Lee, Micro-patterned lithium metal anodes with suppressed dendrite formation for post lithium-ion batteries, Adv. Mater. Interf. 3 (11) (2016) 1600140 http://onlinelibrary.wiley.com/doi/10.1002/admi.201600140/full.

[12] H. Lee, J. Song, Y.-J. Kim, J.-K. Park, H.-T. Kim, Structural modulation of lithium metal-electrolyte interface with three-dimensional metallic interlayer for high-performance lithium metal batteries, Sci. Rep. 6 (2016) 30830 https://www.nature.com/articles/srep30830.

[13] R. Xu, X.Q. Zhang, X.B. Cheng, H.J. Peng, C.Z. Zhao, C. Yan, J.Q. Huang, Artificial soft–rigid protective layer for dendrite-free lithium metal anode, Adv. Funct. Mater. 28 (8) (2018) 1705838 http://onlinelibrary.wiley.com/doi/10.1002/adfm.201705838/full.

[14] X. Liang, Q. Pang, I.R. Kochetkov, M.S. Sempere, H. Huang, X. Sun, L.F. Nazar, A facile surface chemistry route to a stabilized lithium metal anode, Nat. Energy 2 (9) (2017) 17119 https://www.nature.com/articles/nenergy2017119.

[15] K. Yan, Z. Lu, H.-W. Lee, F. Xiong, P.-C. Hsu, Y. Li, J. Zhao, S. Chu, Y. Cui, Selective deposition and stable encapsulation of lithium through heterogeneous seeded growth, Nat. Energy 1 (3) (2016) 16010 https://www.nature.com/articles/nenergy201610.

[16] D. Lin, Y. Liu, Z. Liang, H.-W. Lee, J. Sun, H. Wang, K. Yan, J. Xie, Y. Cui, Layered reduced graphene oxide with nanoscale interlayer gaps as a stable host for lithium metal anodes, Nat. Nanotechnol. 11 (7) (2016) 626 https://www.nature.com/articles/nnano.2016.32.

[17] H. Lee, T. Han, K.Y. Cho, M.-H. Ryou, Y.M. Lee, Dopamine as a novel electrolyte additive for high-voltage lithium-ion batteries, ACS Appl. Mater. Ineterf. 8 (33) (2016) 21366–21372 https://pubs.acs.org/doi/abs/10.1021/acsami.6b06074.

[18] M.-H. Ryou, G.-B. Han, Y.M. Lee, J.-N. Lee, D.J. Lee, Y.O. Yoon, J.-K. Park, Effect of fluoroethylene carbonate on high temperature capacity retention of $LiMn_2O_4$/graphite Li-ion cells, Electrochim. Acta 55 (6) (2010) 2073–2077 https://www.sciencedirect.com/science/article/pii/S0013468609013978.

[19] J.-N. Lee, G.-B. Han, M.-H. Ryou, D.J. Lee, J. Song, J.W. Choi, J.-K. Park, N-(triphenylphosphoranylidene) aniline as a novel electrolyte additive for high voltage $LiCoO_2$ operations in lithium ion batteries, Electrochim. Acta 56 (14) (2011) 5195–5200 https://www.sciencedirect.com/science/article/pii/S0013468611004051.

[20] R. Mogi, M. Inaba, S.-K. Jeong, Y. Iriyama, T. Abe, Z. Ogumi, Effects of some organic additives on lithium deposition in propylene carbonate, J. Electrochem. Soc. 149 (12) (2002) A1578–A1583 http://jes.ecsdl.org/content/149/12/A1578.short.

[21] K. Xu, Nonaqueous liquid electrolytes for lithium-based rechargeable batteries, Chem. Rev. 104 (10) (2004) 4303–4418 http://pubs.acs.org/doi/abs/10.1021/cr030203g.

[22] F. Ding, W. Xu, G.L. Graff, J. Zhang, M.L. Sushko, X. Chen, Y. Shao, M.H. Engelhard, Z. Nie, J. Xiao, Dendrite-free lithium deposition via self-healing electrostatic shield mechanism, J. Am. Chem. Soc. 135 (11) (2013) 4450–4456 http://pubs.acs.org/doi/abs/10.1021/ja312241y.

[23] W. Li, H. Yao, K. Yan, G. Zheng, Z. Liang, Y.-M. Chiang, Y. Cui, The synergetic effect of lithium polysulfide and lithium nitrate to prevent lithium dendrite growth, Nat. Commun. 6 (2015) 7436 https://www.nature.com/articles/ncomms8436.

[24] Y. Zhang, J. Qian, W. Xu, S.M. Russell, X. Chen, E. Nasybulin, P. Bhattacharya, M.H. Engelhard, D. Mei, R. Cao, Dendrite-free lithium deposition with self-aligned nanorod structure, Nano Lett. 14 (12) (2014) 6889–6896 http://pubs.acs.org/doi/abs/10.1021/nl5039117.

[25] F. Ding, W. Xu, X. Chen, J. Zhang, Y. Shao, M.H. Engelhard, Y. Zhang, T.A. Blake, G.L. Graff, X. Liu, Effects of cesium cations in lithium deposition via self-healing electrostatic shield mechanism, J. Phys. Chem. C 118 (8) (2014) 4043–4049 http://pubs.acs.org/doi/abs/10.1021/jp4127754.

[26] H. Xiang, P. Shi, P. Bhattacharya, X. Chen, D. Mei, M.E. Bowden, J. Zheng, J.-G. Zhang, W. Xu, Enhanced charging capability of lithium metal batteries based on lithium bis (trifluoromethanesulfonyl) imide-lithium bis (oxalato) borate dual-salt electrolytes, J. Power Sources 318 (2016) 170–177 https://www.sciencedirect.com/science/article/pii/S0378775316303597.

[27] R. Ahmed, K. Reifsnider, Study of influence of electrode geometry on impedance spectroscopy, Int. J. Electrochm. Sci. 6 (2011) 1159–1174 http://www.electrochemsci.org/papers/vol6/6041159.pdf.

[28] S. Kim, J. Park, A. Friesen, H. Lee, Y.M. Lee, M.-H. Ryou, Composite protection layers for dendrite-suppressing non-granular micro-patterned lithium metal anodes, Electrochim. Acta 282 (2018) 343–350 https://www.sciencedirect.com/science/article/pii/S0013468618311356.